Thermochimica Acta, 174 (1991) 299–320
Elsevier Science Publishers B.V., Amsterdam

LOW FREQUENCY MAGNETIC MEASUREMENTS ON HIGH-T_c SUPERCONDUCTING MATERIALS

FEDOR GÖMÖRY

Institute of Electrical Engineering, Electro-Physical Research Centre, Slovak Academy of Sciences, 842 39 Bratislava (Czechoslovakia)

(Received 26 January 1990)

ABSTRACT

This paper deals with experimental techniques based on analysis of macroscopic magnetic properties of a superconductor placed in a magnetic field varying harmonically with time. Contactless ways of inducing the current into the sample are particularly advantageous in the case of ceramic high-T_c superconductors. Common features of methods utilizing various instrumentation are discussed, as well as differences between models used to determine the parameters characterizing the superconducting material. The usefulness of low-frequency magnetic measurements is demonstrated on a practical example of polycrystalline $YBa_2Cu_3O_x$. Some experimental facts open for theoretical explanation are presented in the last section.

INTRODUCTION

The most familiar feature of a superconductor is the vanishing of its electrical resistance on cooling down to a sufficiently low temperature. Methods allowing us to detect resistance changes can be divided into two groups, differing in the way utilized to raise the current in the sample. In contact methods the sample is electrically connected to a power supply. Another possibility is to induce the current in a contactless way, e.g. by varying the magnetic field with time [1,2]. In this paper, methods based on sensing the voltage response from a pick-up coil surrounding the sample placed in a harmonically varying magnetic field will be discussed.

PRINCIPAL ARRANGEMENT FOR LOW FREQUENCY MAGNETIC MEASUREMENTS ON SUPERCONDUCTORS

The basic experimental arrangement is given in Fig. 1. The pick-up coil is wrapped around the middle region of a cylindrical sample (height $\gg$ diameter). The magnetic field B_{ex}, parallel to the axis of the sample, consists

0040-6031/91/$03.50

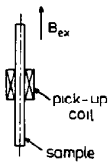

Fig. 1. Basic experimental set-up.

of two parts: the static magnetic field B_d and the a.c. field with amplitude b and frequency $f = \omega/2\pi$

$$B_{ex}(t) = B_d + b \cos \omega t \tag{1}$$

There are no constraints on the upper frequency limit up to $\sim 10^9$ Hz from the point of view of the superconductor. However, in order to avoid parasitic effects in various parts of the apparatus, most researchers work in a frequency region between 10 Hz and 1 kHz.

The cylindrical sample shape mentioned above is the most advantageous one for further evaluation of the quantitative properties of the material. The other well-suited shape is that of a plate with height $\gg$ width $\gg$ thickness, the long axis being parallel to the magnetic field. In these two cases the field acting on the sample is identical to the external field B_{ex}. Using other shapes the induced magnetic moment of the sample cannot be omitted in an evaluation of the field felt by the sample. Sometimes a reasonable estimate can be used, giving the relation between this field and B_{ex} [3,4]. But in general this problem needs a special solution in every particular case.

The voltage in one turn of the pick-up coil is

$$u_i(t) = -\frac{d\phi_{tot}}{dt} \tag{2}$$

given by the time derivative of the linked magnetic flux. Because a gap between the pick-up coil and the sample cannot be avoided in practice, ϕ_{tot} contains the flux in this gap, ϕ_0, plus the flux in the sample, ϕ:

$$\phi_{tot} = \phi + \phi_0 \tag{3}$$

Using some kind of subtraction of the term $d\phi_0/dt$ from the pick-up coil signal we obtained the so-called "compensated" voltage

$$u(t) = -\frac{d\phi(t)}{dt} \tag{4}$$

This voltage contains the most complete information about the magnetization process, spatially averaged over the sample volume roughly corresponding to the pick-up coil bore. There exist numerous ways of processing $u(t)$. As a consequence, there are various methods of studying superconducting materials. The most important will be mentioned below.

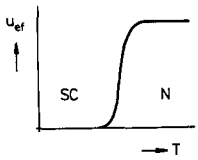

Fig. 2. Inductive measurement of the transition from the normal (N) to the superconducting (SC) state.

Inductive measurement of T_c

For this method, an a.c. voltmeter is used to measure $u(t)$. The instrument gives the effective value

$$u_{ef} = \langle u(t)^2 \rangle^{1/2} \tag{5}$$

where the broken brackets denote a time average. By changing the temperature T one can detect the transition temperature from an abrupt decrease of u_{ef} owing to supercurrents shielding the sample volume against penetration by the magnetic flux. A typical temperature dependence $u_{ef}(T)$ is plotted in Fig. 2.

Alternating current susceptibility measurement

In spite of the fact that the magnetization of a superconducting specimen is generally inhomogeneous, we can introduce a space average of the magnetic field inside the sample $\bar{B}$:

$$\bar{B}(t) = \frac{\phi(t)}{S} \tag{6}$$

where S is the cross-section of the sample. This quantity will follow the external field with some delay owing to energy dissipation during the magnetization. Moreover, superconducting shielding will influence its magnitude. Taking into account only the first harmonics, we can write

$$\bar{B}(t) = B_0 + B_m \cos(\omega t + \varphi) \tag{7}$$

Here, B_0 is a time-independent term corresponding to d.c. magnetization. Alternating current magnetization is represented by a term with amplitude B_m and phase φ regarding the external a.c. field.

The question arises as to how to determine B_m and φ experimentally. A solution is to use a selective amplifier and a phase sensitive detector (PSD) to process $u(t)$. Solving eqn. (4) with the help of eqns. (6) and (7), we obtain

$$u(t) = \omega B_m S \sin(\omega t + \varphi) = u_0 \sin(\omega t + \varphi) \tag{8}$$

Here, $u_0 = \omega S B_m$ is the amplitude of the compensated pick-up coil voltage.

Two output signals of PSD are proportional to $u_0 \cos \varphi$ and $u_0 \sin \varphi$, respectively. It is then possible to calculate

$$\tan \varphi = \frac{u_0 \sin \varphi}{u_0 \cos \varphi}; \qquad B_m = \frac{\left[(u_0 \cos \varphi)^2 + (u_0 \sin \varphi)^2\right]^{1/2}}{\omega S} \tag{9}$$

Let us calculate the time average (with $\tau_0 = 1/f$ being the period of the a.c. field) of the energy supplied by an alternating field into the sample, taking into account eqns. (1) and (7):

$$W_a = \frac{1}{\mu_0 \tau_0} \int_0^{\tau_0} (\bar{B}(t) - B_0)(B_{ex}(t) - B_d)\, dt = \frac{bB_m \cos \varphi}{2\mu_0} \tag{10}$$

Without a sample ($B_m = b$ and $\varphi = 0$) we obtain $W_0 = b^2/2\mu_0$. The difference

$$\Delta W = W_a - W_0 = \frac{b^2}{2\mu_0}\left(\frac{B_m \cos \varphi}{b} - 1\right) \tag{11}$$

reflects the a.c. response of the sample. For the superconductor a shielding effect is typical ($B_m < b$) and $\Delta W < 0$. Calculation of the energy converted to heat during one period of magnetization yields

$$Q = \frac{1}{\mu_0} \oint B_{ex}\, d\bar{B} = -\frac{\pi}{\mu_0} bB_m \sin \varphi \tag{12}$$

From eqns. (11) and (12) one can see that with the help of B_m and φ we can determine the basic energetic quantities of an a.c. magnetization process—the average of the magnetic energy as well as losses.

Another way of describing the relation between an external and internal magnetic field has become more common [5–8]. It is based on the idea of static magnetic susceptibility expressing an internal magnetic field in terms of the external magnetic field:

$$B_{int} = (1 + \chi) B_{ext} \tag{13}$$

Starting from previous calculations, let us introduce two dimensionless quantities

$$\chi' = \left(\frac{B_m \cos \varphi}{b} - 1\right); \qquad \chi'' = -\frac{B_m \sin \varphi}{b} \tag{14}$$

Then

$$\Delta W = \chi' \frac{b^2}{2\mu_0}; \qquad Q = 2\pi\chi'' \frac{b^2}{2\mu_0} \tag{15}$$

χ' and $-\chi''$ could be supposed to be the real and imaginary parts of a complex quantity $\dot{\chi} = \chi' - j\chi''$, where $j = +\sqrt{-1}$. $\dot{\chi}$ is called the complex susceptibility, because owing to eqns. (11), (12) and (14) the relation between symbolic time vectors $\dot{B}_{ex}$ and $\dot{\bar{B}}$ can be expressed as

$$\dot{\bar{B}} = (1 + \dot{\chi}) \dot{B}_{ex} \tag{16}$$

in formal agreement with eqn. (13).

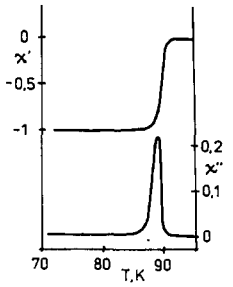

Fig. 3. Temperature dependence of the real and imaginary parts of the a.c. susceptibility.

We have seen in eqns. (8) and (9) that both $B_m \cos \varphi$ and $B_m \sin \varphi$ are present in the output signals of PSD. The only thing we must do to obtain χ' and χ'' is to carry out conversion (14). The angle φ is always $\leqslant 0$, because the losses (eqn. (12)) cannot be negative. For high T_c superconductors having a normal-state resistance which is high enough to neglect eddy currents, the sample does not influence $u(t)$ at $T > T_c$. Then $B_m = b$ and $\varphi = 0$. As a consequence, $\chi'(T > T_c) = 0$ and $\chi''(T > T_c) = 0$. In the Meissner state with perfect shielding $B_m = 0$, and therefore $\chi'(T \ll T_c) = -1$ and $\chi''(T \ll T_c) = 0$. At temperatures slightly below T_c a mixed state occurs, with imperfect shielding and losses due to hysteretic magnetization. Then $-1 < \chi'(T < T_c)$ and $\chi''(T < T_c) > 0$. In Fig. 3 a typical dependence of χ' and χ'' for a $YBa_2Cu_3O_x$ polycrystalline sample [9] is given, showing the behaviour featured above.

Measurement of penetrated and trapped flux

There exists the possibility of allowing PSD to work in a wide band mode, i.e. without selective filtering of the input signal. The input voltage is simply switched in the positive and negative sense, giving the output in-phase signal S' and the output out-of-phase signal S'', respectively:

$$S' = k\left(\int_0^{\tau_0/2} u(t)\,\mathrm{d}t - \int_{\tau_0/2}^{\tau_0} u(t)\,\mathrm{d}t\right) = k[\phi(t=0) - \phi(t=\tau_0/2)]$$

$$S'' = k\left(\int_0^{\tau_0/4} u(t)\,\mathrm{d}t - \int_{\tau_0/4}^{3\tau_0/4} u(t)\,\mathrm{d}t + \int_{3\tau_0/4}^{\tau_0} u(t)\,\mathrm{d}t\right)$$

$$= k(\phi(t=\tau_0/4) - \phi(t=3\tau_0/4)) \qquad (17)$$

Here k is a constant of the instrument, obtainable by measuring the normal-state in-phase response $S'_{nor} = 2\,kbS$.

At $t = 0$ and $t = \tau_0/2$ the a.c. field reaches its maximum. Therefore, S' is proportional to the difference in magnetic fluxes contained in the sample at the positive and negative peak value of the a.c. field. The higher S' is, the

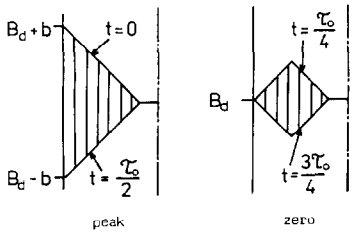

Fig. 4. The magnetic flux contained in the sample (shaded areas) at peak and zero actual values of the a.c. field.

stronger the penetration of the a.c. field into the sample. At $t = \tau_0/4$ and $t = 3\tau_0/4$ the a.c. field is zero, and S'' reflects the ability of the sample to trap some amount of a.c. flux (see Fig. 4). Dividing S' and S'' by the normal state value S'_{nor}, one obtains two dimensionless quantities

$$s' = \frac{S'}{S'_{\text{nor}}}; \qquad s'' = \frac{S''}{S'_{\text{nor}}} \tag{18}$$

s' will be called the normalized penetrated flux and s'' the normalized trapped flux [10].

Let us imagine the transition from the normal to the superconducting state in terms of s' and s''. At $T > T_c$, there is no trapping of the flux penetrating the sample without obstacles. Thus $s'(T > T_c) = 1$ and $s''(T > T_c) = 0$. When the sample reaches the Meissner state, there is neither flux penetration nor flux trapping: $s'(T \ll T_c) = s''(T \ll T_c) = 0$. In between an interval exists with partial shielding of the sample volume by supercurrents. These are hysteretic owing to the pinning of fluxoids on inhomogeneities, thus resulting in flux trapping. These considerations give $0 < s'(T < T_c) < 1$ and $0 < s''(T < T_c)$. In Fig. 5 these types of dependence, obtained experimentally on the same sample as in Fig. 3, are given. Both figures are very similar, when s' is compared with $1 + \chi'$ and s'' is compared with χ''. This is why the couple s' and s'' is sometimes called the "wide band a.c. susceptibility" [11].

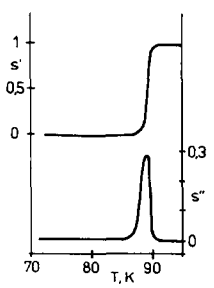

Fig. 5. Temperature dependence of the normalized penetrated (s') and trapped (s'') fluxes.

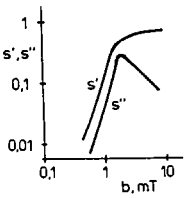

Fig. 6. Amplitude dependence of the normalized penetrated (s') and trapped (s'') fluxes.

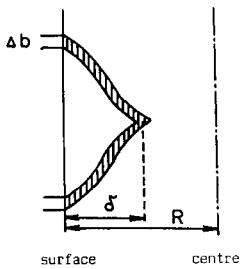

Fig. 7. Increase in the a.c. field penetration enhancing its amplitude b.

Another possibility is to hold the temperature constant, e.g. in a bath of cryogenic liquid, and measure both s' and s'' as functions of b. Such a dependence, measured on the same sample at 77.3 K, is illustrated in Fig. 6. Logarithmic coordinates on both axes enable us to recognize easily the correct compensation of the pick-up coil voltage, indicated by the parallel run of s' and s'' in the low field portion of the plot.

The method of Campbell

This powerful technique is based on analysing the dependence of the in-phase signal S' on the a.c. field amplitude [12]. Its principle is illustrated in Fig. 7. An increase, Δb, in the a.c. field amplitude results in an increase in the penetrated magnetic flux (shaded area)

$$\Delta\left(\phi(0) - \phi(\tau_0/2)\right) = 2\,\Delta b \pi \left(R^2 - (R-\delta)^2\right) \tag{19}$$

The left-hand term can be measured by a phase sensitive detector working in

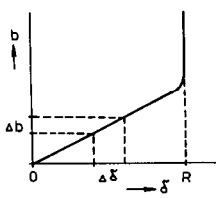

Fig. 8. Relation between the penetration depth and the a.c. field amplitude b.

the wide band mode, and on the right-hand side the depth of the magnetic field penetration, δ, can be found. Let us use the normal-state signal, $S'_{nor} = 2k\pi R^2 b$, to determine the PSD constant k and the sample radius R. Then, replacing differences by derivatives, we obtain

$$\frac{\delta}{R} = 1 - \left(1 - \frac{dS'/db}{dS'_{nor}/db}\right)^{1/2} \tag{20}$$

For the plate-shaped sample this relation is very instructive:

$$\frac{\delta}{a/2} = \frac{dS'/db}{dS'_{nor}/db} \tag{21}$$

Here, $a/2$ is the half-thickness of the plate. As a result of the measurement a graph linking δ with b can be constructed (Fig. 8). From this graph, j_c is calculated

$$j_c = \frac{1}{\mu_0}\frac{\Delta b}{\Delta \delta} \tag{22}$$

where Δb and $\Delta \delta$ are corresponding sections on axes b and δ.

Spatial changes in j_c result in a non-linear shape of the $b(\delta)$ dependence. For every point of such a curve the critical current density at depth δ can be obtained using eqn. (22).

Methods based on analysis of the u(t) waveform

The most complex as well as difficult way of processing the compensated voltage from a pick-up coil is to record and successively analyse it with respect to some particular features [13,14]. These methods helped in the study of important problems related to the pinning of the magnetic flux in type II superconductors. Regarding high-T_c superconductors, in spite of some recent investigations [15] there is lack of complex models reflecting the behaviour of high-T_c superconductors in magnetic fields. Therefore, only one method is mentioned in more detail here, giving as a result the same graph as that in Fig. 8 obtained using Campbell's method.

Using Fig. 7, we can calculate the time-dependent increase in the magnetic flux penetrating into the sample during, for example, an increase in the external field as

$$\Delta\phi(t) = \Delta B_{ex}(t)\left(R^2 - (R-\delta)^2\right)\pi$$

Comparing it with the normal-state increase $\Delta\phi_{nor}(t) = \Delta B_{ex}(T)\pi R^2$, we find the solution for the time-dependent penetration depth is

$$\frac{\delta(t)}{R} = 1 - \left(1 - \frac{d\phi(t)}{d\phi_{nor}(t)}\right)^{1/2} \tag{23}$$

TABLE 1

Comparison of methods

Method	Measured quantity	Key instrument	Variable	Parameters
1 Inductive T_c	u_{ef}	a.c. voltmeter	T	b, B_d, f
2 a.c. susceptibility	χ', χ''	PSD + selected amplifier	T	b, B_d, f
3 Penetrated and trapped flux	s', s''	PSD (2 channel)	b, (T)	T, (b), B_d, f
4 Campbell	(b)	PSD (1 channel)	b	T, B_d, f
5 Voltage analysis	δ, and others	Transient recorder	(Time)	b, B_d, T, f

With both functions, $\phi(t)$ and $\phi_{nor}(t)$, well conditioned, we can rewrite eqn. (23) in the form

$$\frac{\delta(t)}{R} = 1 - \left(1 - \frac{d\phi(t)/dt}{d\phi_{nor}(t)/dt}\right)^{1/2} = 1 - \left(1 - \frac{u(t)}{u_{nor}(t)}\right)^{1/2} \tag{24}$$

This is well suited for analysis of experiments, because it contains $u(t)$ directly [16]. In this method, at a given amplitude b of the a.c. field, the whole field profile curve is obtained; in Campbell's method only one point of it is obtained.

Comparison of the various methods discussed above is given in Table 1, taking into account the measured quantity, key instrument and usual regime of exploitation. The variable quantities change either continuously or stepwise in the measurement. The quantities called parameters, however, need to be held as constant as possible during the experiment. T denotes temperature, b is the a.c. field amplitude and f its frequency, and B_d is the d.c. component of the magnetic field. Following a survey of methods developed for studying superconductor behaviour in a.c. magnetic fields, the question arises as to what can they tell us about the material investigated. The following section should give the answer.

CHARACTERIZATION OF SUPERCONDUCTORS BASED ON LOW-FREQUENCY MAGNETIC MEASUREMENTS

The most important macroscopic parameters which characterize the superconductor are: critical temperature T_c, critical magnetic fields B_{c1}, B_{c2} and B_c, and critical current density j_c. For porous or multi-phase materials, e.g. high-T_c sintered samples, the content of superconducting phase v_g can be of interest.

Critical magnetic fields obtained by various methods for high-T_c materials [17] are rather different. Those based on d.c. magnetization seem to be the most reliable [18]. Alternating current magnetic measurements have not been

shown to be advantageous in this field, therefore only determination of T_c, j_c and v_g will be discussed here.

Critical temperature T_c

To determine the critical temperature, one can use all the methods allowing temperature T as a variable (rows 1, 2 and 3 of Table 1). By measurement on superconductors having a wide transition the criterion of T_c must be well defined. Compared with resistive measurements, where the transition begins at the first superconducting path appearing, a change in $u(t)$ is related to the creation of the first closed superconducting loop. A sample almost filled by critical current density exhibits only about a 50% drop in u_{ef}, s' or χ' compared with the normal state. This fact must be taken into account when comparing T_c measured inductively with that measured resistively.

Critical current density

When determining j_c from inductive measurements (methods listed in rows 2, 3, 4 and 5 of Table 1), we must be aware that this is possible only with the aid of a model. The most simple is that of a spatially homogeneous superconductor in a d.c. field much greater than the a.c. field amplitude. The magnetic field profile is then linear [19] (see Fig. 9). The only problem is to recognize the situation when the a.c. field just reaches the center of the sample. In Fig. 9 this occurred at amplitude b_0.

It has been shown [3,10], that for cylindrical samples the out-of-phase part of the a.c. susceptibility χ'', as well as the normalized trapped flux s'', reaches a maximum under this condition. From the first Maxwell equation in the given geometry one easily obtains

$$j_c(T_0) = \frac{b_0}{\mu_0 R} \tag{25}$$

Here, the temperature at which the field of amplitude b_0 just reaches the centre of the sample was called T_0.

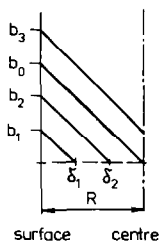

Fig. 9. Magnetic field profiles at $t = 0$ inside a superconducting cylinder with j_c = constant.

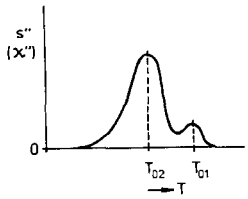

Fig. 10. Temperature dependence of s'' for a high-T_c superconductor with intergrain and intragrain supercurrents.

With the help of methods giving a relation between the penetration depth δ and the a.c. field amplitude b, j_c can be obtained using eqn. (21), see Fig. 8.

It is well known that in high-T_c superconductors two types of supercurrents exist [20–23]. For the elementary coherent volume, called the grain, the intragranular critical current density is characteristic. In the sample as a whole the shielding as well as the transport current carrying capacity is determined by the macroscopic intergranular critical current density. Owing to a significant difference in the order of magnitude of these two types of supercurrents, their effects are separable in low-frequency magnetic measurements.

As a consequence, two peaks occur in the temperature dependence plot of χ'' or s'' [8]. At a sufficiently low temperature the sample is shielded by intergranular currents. On increasing the temperature the intragranular j_c decreases, and at T_{02} the a.c. field reaches the centre of the sample, see Fig. 10. At this temperature, intragranular currents almost completely shield the grains. With a further temperature increase, intergranular currents become negligible and the a.c. field begins to penetrate the grains. At T_{01}, the centre of an average grain is reached by the a.c. field. In this way, from the curve schematically drawn in Fig. 10, the intergranular critical current density j_{cg} at temperature T_{01} can be calculated.

$$j_{cm}(T_{02}) = \frac{b_0}{\mu_0 R} \tag{26a}$$

$$j_{cg}(T_{01}) = \frac{b_0}{\mu_0 R_g} \tag{26b}$$

Note that in eqn. (26b) the average grain radius R_g is used instead of that of the sample.

Owing to the existence of the critical current densities the field profile curve is composed of two parts (Fig. 11). At low a.c. amplitudes the grains are screened well and the field penetrates into intergranular regions, shielded by the intergranular critical current density. At the amplitude b^*, the whole

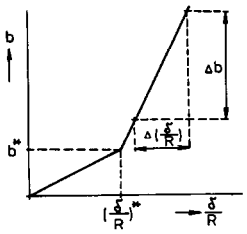

Fig. 11. Field profile curve for a high-T_c superconductor composed of two parts owing to the existence of two types of supercurrents.

intergranular volume is just penetrated and the intergranular critical current density can be calculated

$$j_{cm} = \frac{b^\star}{\mu_0 R} \tag{27}$$

This is a macroscopic characteristic, related to the total volume of the sample. On increasing the a.c. field further, it begins to penetrate into the grains. In this way, from the right-hand side of Fig. 11, the intergranular current density is determined using the slope $\Delta b/\Delta(\delta/R)$:

$$j_{cg} = \frac{1}{\mu_0 R_g} \frac{\Delta b}{\Delta(\delta/R)} \tag{28}$$

The whole measurement is carried out at a fixed temperature, T_0, to which the critical current densities calculated are ascribed.

Volume content of superconductor v_g

As in the previous section, the model of a constant macroscopic critical current density will aid us. This model is not far from reality when $B_d \gg b$. In the considerations that follow we assume this condition to be fulfilled. Because the intragranular current density is much higher than the intergranular one, the grains are well shielded at a.c. fields just penetrating the intergranular volume. Therefore, we can replace them by diamagnetic particles embedded in a matrix of type II superconductor. The theoretical height of the s'' maximum for a type II superconductor is 0.25 (cylinder) or 0.295 (slab) [10]. With the volume fraction v_g occupied by diamagnetic particles, the trapped magnetic flux will be accordingly lower (see Fig. 12). Comparing the actual value s_0'' of the maximum in the s'' curve with the theoretical value $s_{0,th}''$ one can calculate the volume occupied by the diamagnetic particles, V_g, in the ratio to the sample total volume V_{tot}:

$$v_g = \frac{V_g}{V_{tot}} = 1 - \frac{s_0''}{s_{0,th}''} \tag{29}$$

Similar considerations can be made concerning the field profile curves. At $b = b^\star$ all the intergranular volume is filled by magnetic flux. Without

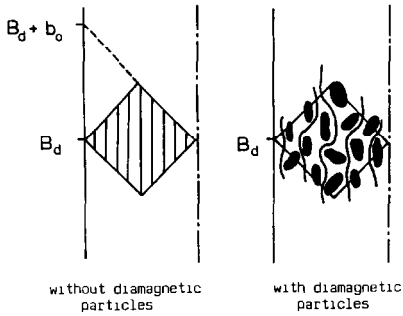

Fig. 12. Decrease in the trapped magnetic flux caused by diamagnetic particles spread in the sample.

diamagnetic particles inside, the penetration depth should be $\delta = R$ at that moment. The fact that correspondingly $(\delta/R)^\star < 1$ reflects the presence of diamagnetic grains in the sample. In the case of a cylindrical sample we obtain

$$v_g = [1 - (\delta/R)^\star]^2 \tag{30a}$$

and for a slab

$$v_g = 1 - \left(\frac{\delta}{a/2}\right)^\star \tag{30b}$$

Practical example

In order to demonstrate the utility of low-frequency magnetic measurements the results obtained on a typical $YBa_2Cu_3O_x$ polycrystalline sample are presented here. The sample was cylindrical, with diameter 1.9 mm and height 12 mm. The mass density of the sample was 5.4 g cm^{-3}. X-ray analysis showed it was single phase orthorhombic [9]. The features incorporated in the measuring apparatus in order to enhance the precision and reproducibility of measurements were:

(1) d.c. and a.c. magnetic fields were generated by different solenoids, magnetically decoupled by an additional inductance in the d.c. solenoid circuit.

(2) The pick-up coil was wound directly around the sample. Only about 15% of the signal was to be compensated when the sample was superconducting.

(3) The thermometer in a non-metallic case was attached directly to the sample thermal contact being enhanced by silicone grease.

(4) The a.c. solenoid was wound from copper cable composed of isolated strands in order to depress eddy current effects.

(5) The measurements were performed in an LN_2 nonmetallic horizontal cryostat, with the d.c. solenoid kept at almost constant temperature. The

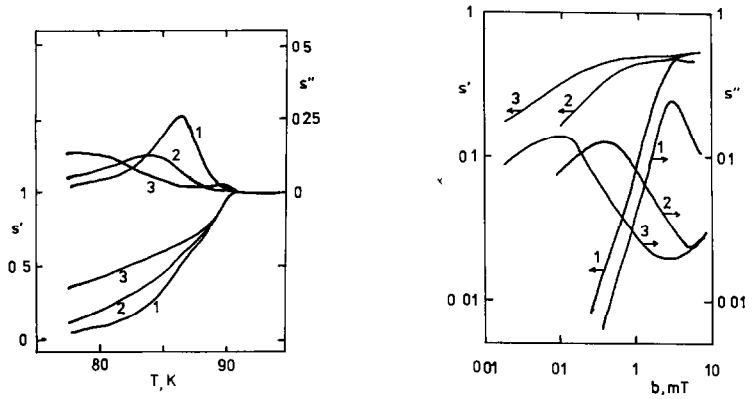

Fig. 13. a, Temperature dependence of the penetrated (s') and trapped (s'') magnetic fluxes measured on a $YBa_2Cu_3O_x$ polycrystalline sample. Amplitude of a.c. field b, 0.85 mT. Superimposed d.c. field: 1, 0; 2, 2 mT; 3, 5 mT. b, Amplitude dependence of the penetrated (s') and trapped (s'') magnetic fluxes for the same sample at $T = 77.3$ K. Superimposed d.c. field: 1, 0; 2, 5 mT; 3, 10 mT.

temperature of the sample was controlled either by changing the level of liquid or by heating the sample holder.

(6) The mutual inductance used to compensate the superfluous signal from the pick-up coil was placed outside the cryostat, at ambient temperature.

In Fig. 13a the temperature dependences of the penetrated and trapped flux, measured at an ac field amplitude $b = 0.85$ mT at three different d.c. fields are plotted. The transition starts at $T_{on} = 91$ K. In the interval between approximately 89 K and 91 K, only the grains are superconducting [23]—s' is the same for the three d.c. fields owing to the high B_{c2} of the grain material. In the same temperature interval, the trapped flux is nearly zero for $B_d \leqslant 2$ mT, indicating reversible flux motion. Below 87 K, the curves are evidently different. In this region macroscopic screening of the whole sample is realized by intergranular currents. They depend substantially on the d.c. magnetic field, and as a consequence various s' and s'' curves are measured at different B_d.

Amplitude dependences of the penetrated and trapped magnetic flux measured at 77.3 K are shown in Fig. 13b. Besides the curves measured at $B_d = 0$, those registered at two non-zero d.c. fields are presented. Only intergranular peaks are visible at the a.c. field amplitudes achievable.

From the series of curves similar to those illustrated in Fig. 13 the intergranular critical current density and its dependence on temperature and magnetic field can be obtained. To do this the intergranular maxima of $s''(t)$ and $s''(b)$ must be identified with the subsequent application of eqn. (26a). Results of such a procedure are given in Figs. 14 and 15. One can conclude that the macroscopic current in our sample is governed by weak

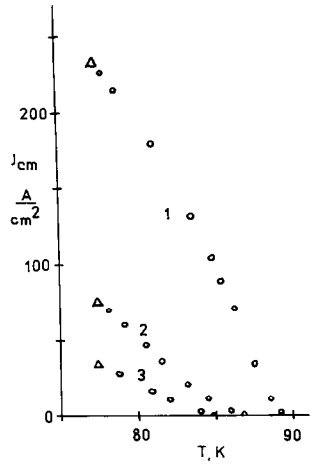

Fig. 14. Temperature dependence of the macroscopic critical current density j_{cm} in a $YBa_2Cu_3O_x$ polycrystalline sample determined from measurement of the trapped magnetic flux s'' at constant a.c. field amplitude (circles) and at constant temperature (triangles). Superimposed d.c. field: 1, 0; 2, 5 mT; 3, 10 mT.

links, their nature being described by the microbridge model [24]. The striking feature observed for polycrystalline Y–Ba–Cu–O is the difference between the macroscopic critical current density observed when cooling the sample in a d.c. field (so-called field cooling, FC), unlike cooling in zero field with subsequent applying of a d.c. field (zero field cooling, ZFC). It is important to use some defined measurement sequence in order to obtain reproducible and comparable results.

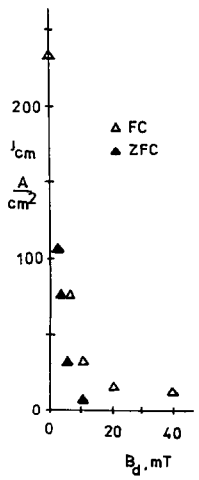

Fig. 15. Dependence of the macroscopic critical current density j_{cm} on the d.c. field, determined for the same sample as in Fig. 14 from measurement of the trapped magnetic flux s'' at $T = 77.3$ K.

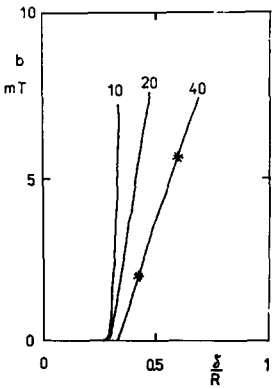

Fig. 16. Field profiles in a $YBa_2Cu_3O_x$ polycrystalline sample at 77.3 K, constructed according to Campbell's method. The intergrain portion of the curves is virtually invisible.

Typical field profiles constructed according to Campbell's procedure are illustrated in Fig. 16. Only the intergranular part of the profiles is visible for the scaling of the axes given. Identifying the starting points of the curves with $(\delta/R)^{\star}$, we can calculate the content of superconducting grains using eqn. (30a). For $B_d = 10$ as well as 20 mT, $(\delta/R)^{\star} = 0.3$ yielding a 49% content of superconducting grains. At $B_d = 40$ mT, $(\delta/R)^{\star} = 0.35$ and the v_g value decreases to 42%. We compare these numbers with those calculated from the maxima of the trapped magnetic flux. From Fig. 12 we can determine $s_0''(T) = 0.135$ and from Fig. 13 $s_0''(b) = 0.143$. Using eqn. (29) one calculates $v_g = 46\%$ and $v_g = 43\%$, respectively. Good agreement between results obtained in different ways demonstrates that appropriate models have been utilized.

The slope of the $b(\delta/R)$ curves in Fig. 16 could be used to determine the intragranular critical current densities. The main difficulty is the uncertainty about the grain radius R_g. Several investigations have shown that the elementary coherent superconducting volume is not identical with the grain observed by optical methods [25]. To make the use of the method clear, we assume, for example, that $R_g = 5$ μm. From the section between the two asterisks on the profile measured at $B_d = 40$ mT we find $\Delta(\delta/R) = 0.2$ and $\Delta b = 4.5$ mT. Inserting these values into eqn. (28) gives $j_{cg} = 3.6 \times 10^5$ A/cm^{-2}.

A question can naturally arise concerning the correctness of the parameters and the properties obtained with the help of low-frequency magnetic measurements. To check it, an experiment with a set of $YBa_2Cu_3O_{7-x}$ samples has been performed [9]. The samples were sintered at different temperatures, which leads to variations in macroscopic properties. In Fig. 17 a comparison of the macroscopic critical current densities obtained resistively, $j_{c,rez}$, with those obtained from s'' curves (j_{cm}) is given. The correlation coefficient is $r = 0.87$. Such agreement is quite surprising, taking into

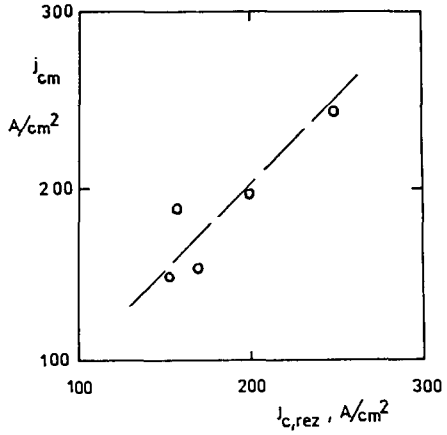

Fig. 17. Comparison of critical current densities obtained resistively ($j_{c,rez}$) with those determined from trapped flux maxima on a set of polycrystalline $YBa_2Cu_3O_x$ samples.

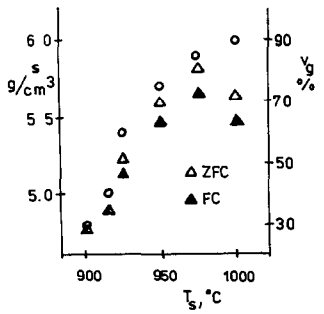

Fig. 18. Correlation between the mass density s (circles) and the volume fraction of superconducting grain v_g (triangles) at 77.3 K for a set of Y–Ba–Cu–O samples.

account the fact that the contactless method should not work well in a zero d.c. field. In Fig. 18, mass densities as well as the volume content of the superconductor, v_g, for the set of samples are given as a function of the sintering temperature. One can see that up to $T_s = 975\,°C$ both quantities are strongly correlated. Above 975 °C partial decomposition of $YBa_2Cu_3O_7$ takes place, resulting in an increase in the mass density with a simultaneous decrease in the superconducting volume portion.

STUDY OF OTHER SUPERCONDUCTING PROPERTIES

To attract the reader's attention to other problems where inductive low-frequency magnetic measurements can be of use, some interesting experimental facts are briefly described.

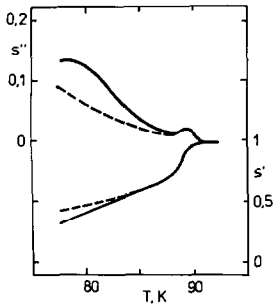

Fig. 19. Difference between field cooling (———) and zero field cooling (– – –) values of the penetrated and trapped magnetic fluxes, measured on a polycrystalline $YBa_2Cu_3O_7$ sample. a.c. field amplitude, 1 mT; d.c. field, 5 mT.

ZFC–FC difference

Figure 19 shows a comparison between ZFC and FC curves of penetrated and trapped flux, measured on polycrystalline bulk $YBa_2Cu_3O_7$. It may be clearly seen that the difference concerns intergranular currents only. On equivalent curves measured on a polycrystalline Bi(Pb)–Sr–Ca–Cu–O [26] sample (Fig. 20) one can see that the difference is hardly noticable. Tl–Ca–Ba–Cu–O samples behaved similarly [27]. It is evident that besides the critical temperature some other essential difference exists between yttrium-based samples on the one hand and bismuth- or thallium-based samples on the other. Its origin has not been explained clearly yet, although structural (twin planes) as well as electromagnetic (flux lines lattice melting [28]) reasons may be responsible.

Relaxation and viscous effects

Magnetization experiments on classical low-temperature superconductors exhibit purely hysteretic character owing to a negligible value of the viscos-

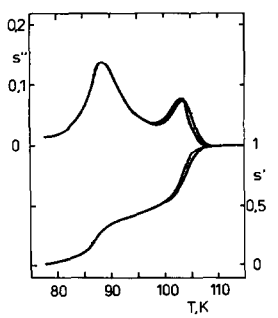

Fig. 20. FC–ZFC couple of s' and s'' measured in the same circumstances as in Fig. 19 on a Bi(Pb)–Sr–Ca–Cu–O sample. The FC and ZFC curves are practically identical.

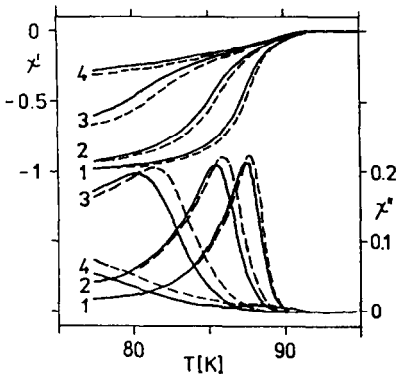

Fig. 21. a.c. susceptibility curves measured at various d.c. and a.c. (peak values) fields on polycrystalline Y–Ba–Cu–O: 1, 0.08 mT a.c.; 2, 0.08 mT a.c. + 2 mT d.c.; 3, 0.08 mT a.c. + 10 mT d.c.; 4, 0.8 mT a.c. + 10 mT d.c. ———, 29 Hz; – – –, 290 Hz.

ity force acting on the fluxoid in motion. Theoretical considerations for high-T_c superconductors lead to an expected large influence of the viscous flux flow [29]. Experimentally this should be measurable, e.g. as a frequency dependence of the a.c. susceptibility. Results of our investigations are illustrated in Fig. 21. A difference of one order of magnitude in frequency has caused only a slight change in the $\chi'(T)$ and $\chi''(T)$ curves. Experiments of this type are very difficult to carry out, because various parasitic effects originating in eddy currents in the metallic parts as well as impedance changes of capacitive connections must be kept at a negligible level over the whole frequency range used. From Fig. 21 one can conclude that the frequency dependence is much weaker than expected. Possible explanations involve the flux transport realized by Josephson vortices instead of Abrikosov vortices in high-T_c superconductors [30] and the flux at grain boundaries [31].

Anisotropy of j_c

Early studies on single crystal $YBa_2Cu_3O_7$ have reported a strong anisotropy of the critical current density. Unfortunately, single crystals of this material have the shape of thin plates, causing difficulties in the quantitative evaluation of the experimental results. In Figs. 22 and 23 $s'(T)$ and $s''(T)$ measured on $YBa_2Cu_3O_7$ single crystals prepared at the University of Bordeaux [32] are presented. When placing the sample parallel to B_{ex} (in this way B_{ex} is perpendicular to c) a picture similar to that obtained for polycrystalline Y–Ba–Cu–O (i.e. with weak link effects) was observed. For the measurement with B_{ex} parallel to c a flat pick-up coil with inner diameter 1 mm and outer diameter 2 mm was attached to the sample placed perpendicularly to B_{ex}. In this configuration the field acting on the sample

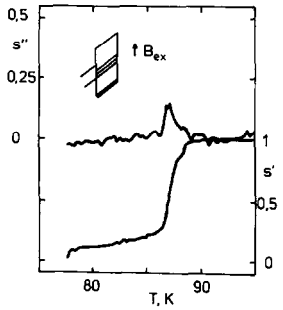

Fig. 22. Temperature dependence of the penetrated and trapped fluxes measured on a $YBa_2Cu_3O_7$ single crystal. a.c. field (amplitude 0.05 mT) perpendicular to the c axis, zero dc.

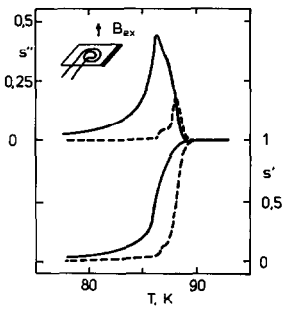

Fig. 23. The same dependence for B_{ex} parallel to the c axis. a.c. field amplitudes: – – –, 0.01 mT; ———, 0.1 mT. Zero superimposed d.c. field.

exceeds B_{ex} many times and the determination of j_{cm} is impossible. However, at a.c. field amplitudes lower than 0.01 mT the temperature interval with perfect screening of the sample is visible.

CONCLUSIONS

Low-frequency magnetic measurements represent a family of powerful techniques for the study of classical and, especially, high-T_c superconductors. There exist various methods differing in such aspects as instrumentation price, duration of the experiment, simplicity of evaluation, and complexity of the material's characterization. Because contacts are unnecessary these methods are well suited to obtain information from various stages of sample preparation and to study the influence of technological parameters on the end product. Of course, parallel use of other methods (resistive, d.c. magnetization, structural analysis, etc.) is recommended to avoid misinterpretation of the effects observed for the first time. I believe that low

frequency magnetic measurements will contribute to solving numerous current problems in the field of high-T_c superconductivity.

ACKNOWLEDGEMENTS

I would like to express my thanks to numerous colleagues for their collaboration in investigations allowing me to prepare this paper. The apparatus was built with a substantial contribution by P. Lobotka. Many theoretical aspects of the experimental methods and results were explained with the help of L. Cesnak and S. Takács. Various samples were kindly provided by V. Plecháček and must be acknowledged too, as well as useful comments from Š. Beňačka, I. Hlásnik and K. Fröhlich.

REFERENCES

1 H. Ullmaier, Irreversible Properties of Type II Superconductors, Springer-Verlag, Berlin, 1975, p. 125.
2 A.M. Campbell and J.E. Evetts, Critical Currents in Superconductors, Taylor and Francis, London, 1972, p. 119.
3 F. Gömöry and P. Lobotka, Solid State Commun., 66 (1988) 645.
4 R.B. Goldfarb and J.V. Minervini, Rev. Sci. Instrum., 55 (1984) 761.
5 E. Maxwell and M. Strongin, Phys. Rev. Lett., 10 (1963) 212.
6 M. Couach, A.F. Khoder and F. Monnier, Cryogenics, 25 (1985) 695.
7 T. Ishida and H. Mazaki, Jpn. J. Appl. Phys., 26 (1987) L1296.
8 R.B. Goldfarb, A.F. Clark, A.I. Braginski and A.J. Panson, Cryogenics, 27 (1987) 475.
9 F. Gömöry, S. Takács, P. Lobotka, K. Fröhlich and W. Plecháček, Physica C, 160 (1989) 1.
10 F. Gömöry, Solid State Commun., 70 (1989) 879.
11 P. Dubots and J.Cave, Cryogenics, 28 (1988) 661.
12 A.M. Campbell, J. Phys. C, 2 (1969) 1492.
13 D. Eckert and A. Handstein, Phys. Status Solidi A, 37 (1976) 171.
14 H.A. Ullmaier, Phys. Status Solidi A, 17 (1966) 63.
15 K.H. Müller, J.C. Macfarlane and R. Driver, Physica C, 158 (1989) 366.
16 R.W. Rollins, H. Küpfer and W. Gey, J. Appl. Phys., 45 (1974) 5329.
17 A.K. Grover, C. Radhakrishnamurty, P. Chaddah, G. Ravi Kumar and G.V. Subba Rao, Pramana, 30 (1988) 569.
18 H.W. Weber, in Studies of High Temperature Superconductors, Nova, 1989.
19 C.P. Bean, Rev. Mod. Phys., 36 (1964) 31.
20 H. Küpfer, I. Apfelstedt, R. Flükiger, R. Meier-Hirmer, W. Schauer, T. Wolf and H. Wühl, presented at the International Discussion Meeting on High-T_c Superconductors, Mautendorf, 7–11 February 1988.
21 H. Küpfer, I. Apfelstedt, R. Flükiger, C. Keller, R. Meier-Hirmer, R. Runtsch, A. Turowski, U. Weich and T. Wolf, Cryogenics, 28 (1988) 650.
22 J. Garcia, C. Rillo, F. Lera, J. Bartolome, R. Navarro, D.H.A. Blank and J. Flokstra, J. Magn. Magn. Mater., 69 (1987) L225.
23 J.R. Glem, Physica C, 153–155 (1988) 50.

24 O. Kulik and A.N. Omelyanchuk, Sov. J. Low-Temp. Phys., 3 (1977) 459.
25 D.C. Larbalestier, S.E. Babcock, X. Cai, L. Cooley, M. Daumling, D.P. Hampshire, J. McKinnell and J. Seutjens, Tokai University Symposium on Superconductivity, November 1988.
26 V. Plecháček and F. Gömöry, Solid State Commun., 73 (1990) 349.
27 J. Tóth personal communication.
28 B. Batlogg, presented at the Experimental Workshop on High-T_c Superconductors, Tricste, 1989.
29 S. Takács and F. Gömöry, Superconductor Sci Technol., 3 (1990) 94.
30 Š. Beňačka, private communication.
31 M. Nikolo and R.B. Goldfarb, Phys. Rev. B, 39 (1989) 6615.
32 L. Nganga, V. Huong Pham, J.P. Chaminade, J.P. Dorder, K. Früylich and M. Jergel, presented at European Materials Research Society Symposium A, Strassbourg, 1990.